AIAA JOURNAL
Vol. 41, No. 8, August 2003

Nonaxisymmetrical Fuselage Shape Modification for Drag Reduction of Low-Sonic-Boom Airplane

Yoshikazu Makino,* Ken'ichiro Suzuki,† Masayoshi Noguchi,‡ and Kenji Yoshida§
National Aerospace Laboratory, Tokyo 182-8522, Japan

The effects of nonaxisymmetrical fuselage design for reducing the drag of a low-sonic-boom airplane are investigated by computational fluid dynamics (CFD) analyses and verified in wind-tunnel tests. The nonaxisymmetrical fuselage design, in which the upper side of a fuselage is designed for low drag whereas the lower side is designed for low sonic boom, is applied to the design of a Mach 1.7 scaled supersonic experimental airplane. The designed airplane is compared with a low-drag airplane and a low-sonic-boom airplane with an axisymmetrical fuselage. The CFD analyses show the nonaxisymmetrical fuselage design can significantly reduce the drag of a low-sonic-boom airplane with an axisymmetrical fuselage without losing its low-sonic-boom characteristics. The CFD results are verified by force and near-field pressure measurements in supersonic wind-tunnel tests.

Nomenclature

A_e	=	equivalent-area distribution of airplane
C_D	=	drag coefficient
C_{Dp}	=	pressure drag coefficient
C_L	=	lift coefficient
C_p	=	pressure coefficient
$F(\tau)$	=	F function
H	=	normal distance from airplane
K_R	=	ground reflection factor of sonic boom
L	=	airplane length
M	=	Mach number
p	=	static pressure
p_∞	=	freestream static pressure
x	=	axial coordinate of airplane
y_f	=	nose bluntness relaxation parameter
α	=	angle of attack
β	=	$\sqrt{(M^2-1)}$
γ	=	specific heat ratio
Δp	=	shock overpressure
μ	=	Mach angle

Introduction

THE National Aerospace Laboratory (NAL) of Japan started a scaled supersonic experimental airplane program[1] in 1996. The main objective of this project is to establish advanced airplane drag reduction technologies including computational fluid dynamics (CFD)-based total design tools for an economically feasible next generation supersonic transport (SST). As well as the drag minimum design, the design for reducing the sonic-boom caused by supersonic overland flight is important for an environmentally feasible SST. Many kinds of low-sonic-boom design methods have been published. Seebass and George[2] determined the equivalent area distribution of the airplane that minimized the sonic-boom intensity. However, the area distribution has an extremely blunt nose shape, which produces large drag. Therefore, a tradeoff between airplane drag and sonic-boom intensity is needed. Darden[3] modified the Seebass–George[2] sonic-boom minimization method to reduce the drag by controlling the bluntness of the area distribution near the nose.

In this study, a nonaxisymmetrical fuselage design is used in the low-sonic-boom design to avoid the drag penalty. The major objective of this paper is a verification of the nonaxisymmetrical fuselage design concept for reducing the drag of a low-sonic-boom airplane with an axisymmetrical fuselage without losing its low sonic-boom characteristics.

Low-Drag/Low-Boom Design Method

Darden's low-boom design[3] is based on the F-function method,[4] which is a modified linear theory developed by Whitham for predicting the sonic boom. In the F-function method, the perturbation pressure is given by

$$(p - p_\infty)/p_\infty = \left[\gamma M^2 \Big/ \sqrt{2\beta(H/L)}\right] F(\tau) \tag{1}$$

The F function $F(\tau)$ can be expressed as

$$F(\tau) = \frac{1}{2\pi} \int_0^\tau \frac{Ae''}{\sqrt{\tau - t}}\, \mathrm{d}t \tag{2}$$

In Darden's low-boom design method,[3] the F function is defined by several parameters that have an influence on the shape of the ground pressure signature or the sonic-boom intensity. One of these parameters, y_f, controls the nose bluntness of the airplane. The airplane has a blunt nose when y_f is small. Darden's low-boom design method only provides the total equivalent area distribution of the airplane, which consists of two basic components: the actual area of the configuration and the equivalent area due to the distribution of lift. The actual area at a given point on the flight-path axis is determined by a frontal projection of the cross-sectional area of the configuration intercepted by a cutting plane inclined forward at the angle of $\pi/2 - \mu$ from the cutting plane normal to the body axis. The equivalent area due to the distribution of lift is determined by a summation of a local force per unit longitudinal distance.[5] Therefore, there are infinite combinations of the fuselage and wing geometries that have the same total equivalent area distribution. In the low-boom design of the experimental airplane in this study, the main wing is determined for drag reduction, and only the fuselage geometry is modified for boom minimization. The equivalent area due to the distribution of lift and the actual areas of the airplane components except the fuselage are subtracted from the target low-boom area distribution determined by Darden's method.[3] The rest

Received 24 September 2002; presented as Paper 2003-0557 at the 41st AIAA Aerospace Sciences Meeting, Reno, NV, 6–9 January 2003; revision received 17 March 2003; accepted for publication 6 April 2003.

*Senior Researcher, Next Generation Supersonic Transport Project Center, 7-44-1 Jindaiji.higashi, Chofu. Member AIAA.
†Aerospace Research Associate, Next Generation Supersonic Transport Project Center, 7-44-1 Jindaiji.higashi, Chofu.
‡Senior Researcher, Next Generation Supersonic Transport Project Center, 7-44-1 Jindaiji.higashi, Chofu.
§Group Leader, Next Generation Supersonic Transport Project Center, 7-44-1 Jindaiji.higashi, Chofu. Member AIAA.

of the area distribution is for the low-boom designed fuselage. If the fuselage is axisymmetrical, its geometry is directly determined from the area distribution. The fuselage geometry considered in this study, however, is not directly determined from the area distribution because the design space of the fuselage is expanded to a nonaxisymmetrical geometry for low-drag/low-boom concept. The idea of the nonaxisymmetrical fuselage is that the lower side of the fuselage of the airplane, which seems to have a big influence on the sonic boom, is designed for low-boom, whereas the upper side of the fuselage is designed for low drag.

Design Result

Airplane Configuration Without Nacelles

The experimental airplane in the preliminary design phase is shown in Fig. 1. The nacelles are big for such a scaled airplane because we plan to use two existing engines for its propulsion system. The airplane length is 11.5 m, and the span is 4.93 m. For a simple design test, the nacelles are not considered in this section. The low-drag/low-boom design method is applied to a main wing, fuselage, and tail wing configuration shown in Fig. 2. The main wing and tail wing geometries are the same as shown in Fig. 1. The baseline configuration shown in Fig. 2a is called the low-drag configuration and is compared with the other two configurations in this section. The axisymmetrical fuselage of the low-drag configuration, which is extended to 12 m, is newly designed for this case by an area rule so that its circumferentially averaged area distribution[6] coincides with a Sears–Haack body area distribution shown in Fig. 3. The fuselage of the low-drag configuration is replaced by a low-sonic-boom designed fuselage to define the low-boom configuration shown in Fig. 2b. In the low-sonic-boom design, a flattop-type low-sonic-boom signature is prescribed as a target pressure signature, and the nose bluntness of a fuselage is relaxed to suppress drag increase by setting the parameter y_f at 0.1. The total equivalent area distribution of the low-boom configuration is shown in Fig. 4 compared with the target area distribution defined by Darden's method.[3] The total equivalent area distribution shows good agreement with the target before $x = 8$ m. However, it is different from the target in the rear part because the wing planform is not designed for a low-sonic-boom concept, that is, the equivalent area distribution due to lift is about the same as that of the low-drag configuration. It means that the reduction of a rear shock intensity of the sonic-boom signature is not taken into account in this low-sonic-boom design. Therefore, sonic-boom intensities are defined by the initial pressure rises of the ground pressure signatures in this study. A nonaxisymmetrical fuselage design is applied to the low-boom configuration. In the design, a fuselage geometry is defined by the upper, side, and lower fuselage radius distributions along an airplane axis. Therefore, a cross section of the fuselage is composed of upper- and lower-half ellipses. The side and lower radius distributions are determined from the same low-sonic-boom target area distribution as the low-boom configuration, whereas the upper radius distribution is fixed to that of the low-drag configuration. The designed configuration is shown in Fig. 2c and is called the low-drag/low-boom configuration.

A three-dimensional Euler CFD code estimates pressure drag coefficients of these three configurations. As an example, the CFD analysis for the low-drag configuration is shown in Fig. 5. The number of grid points used in this CFD analysis is about 3.5 million. The grid outer boundary and the downstream grid surface are extended outward from the body axis to capture shock waves as sharply as possible at some distance from the airplane. Details of the CFD code used in this study are given in Ref. 7, and the CFD results are compared with experimental data for validation in Ref. 8. In the near-field pressure field shown in Fig. 5b, two shocks from

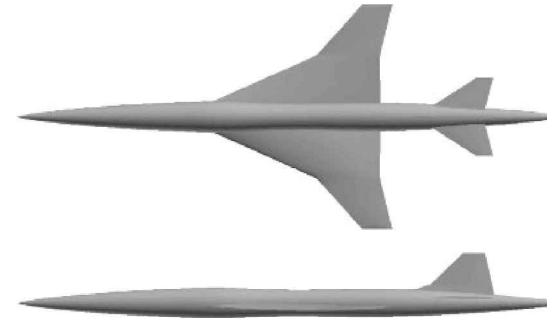

a) Low-drag configuration

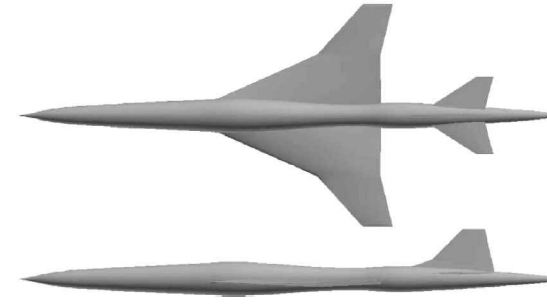

b) Low-boom configuration

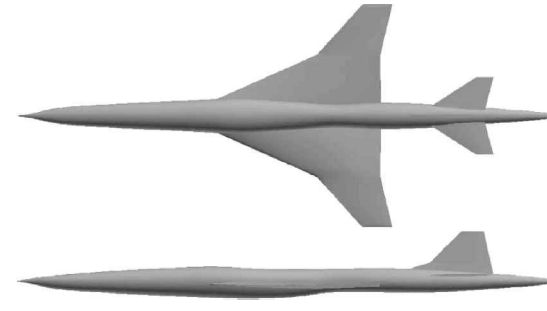

c) Low-drag/low-boom configuration

Fig. 2 Airplane configurations without nacelles.

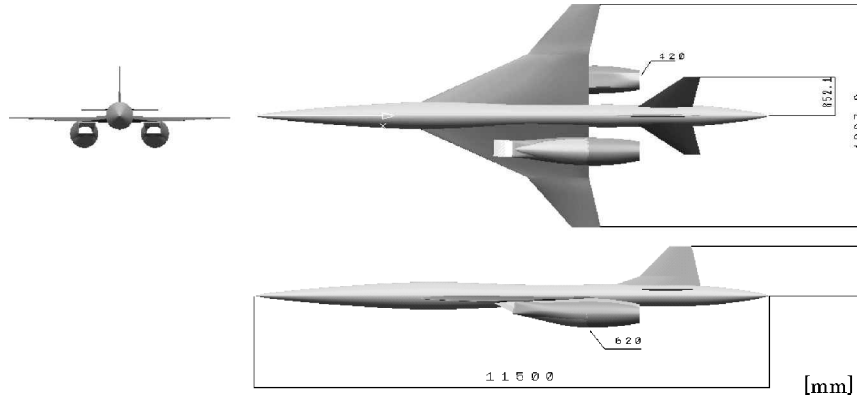

Fig. 1 Jet-powered experimental airplane.

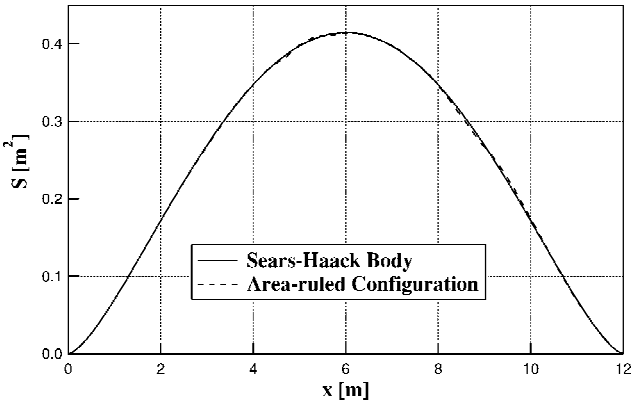

Fig. 3 Area distribution of low-drag configuration without nacelles.

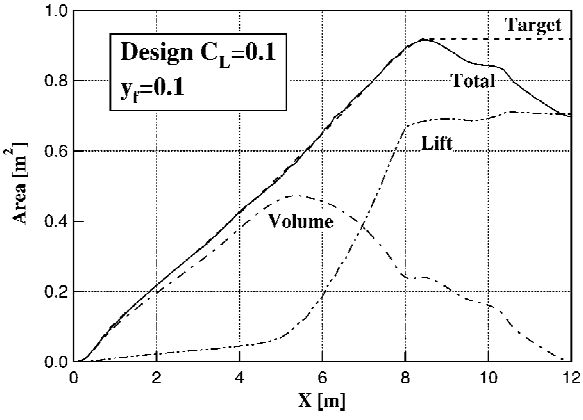

Fig. 4 Equivalent area distribution of low-boom configuration without nacelles.

the nose and wing are clearly seen under the airplane. These two shocks generate two peaks in the near-field pressure signature at two times the airplane length under the airplane shown in Fig. 6. On the other hand, pressure signatures for the low-boom and low-drag/low-boom configurations show the flattop-like shape in the front part, and the peaks due to the wing shock are much lower than that for the low-drag configuration. These near-field pressure signatures are extrapolated to the ground by the waveform parameter method[9] to predict sonic-boom pressure signatures. The F-function method and the waveform parameter method are mathematically equivalent because both methods utilize geometric acoustics and isentropic wave theory. The waveform parameter method requires several input data such as flight conditions and atmospheric properties. The following input data are used here: flight Mach number of 1.7, flight altitude of 15 km, and standard no-wind atmospheric conditions. A reflection factor K_R on the ground is 1.9 in this study. The position of a near-field pressure signature used as an input data for the waveform parameter method is important for predicting sonic-boom intensity on the ground. It is needed to use the near-field signature at a certain distance from an airplane to take into account the three-dimensional airplane configuration effects, although the shock wave itself is difficult to be captured sharply in the CFD analysis. In this study, a near-field pressure signature at $H/L = 2.0$ (two times the airplane length under the airplane) is selected for an input signature because it is shown that the ground pressure signatures extrapolated from the near-field pressure signatures at $H/L = 2.0$ or farther are about the same.

The extrapolated ground pressure signatures for the three configurations are also shown in Fig. 6. The ground signature for the low-drag configuration becomes a typical N-shaped signature, whose initial pressure rise is about 22.5 Pa (0.47 psf) and duration time is about 53 ms. The predicted sonic-boom signature is much weaker than that for the Concorde (initial pressure rise 100 ~ 150 Pa with duration time 200 ms) because the scaled airplane is about 1/5 as

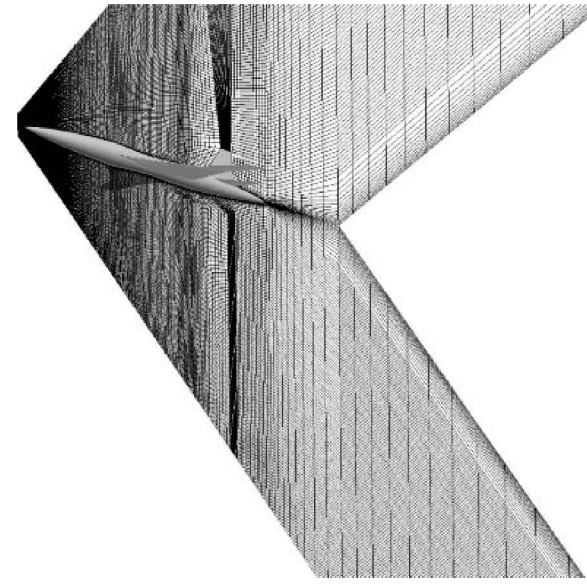

a) Computational grid

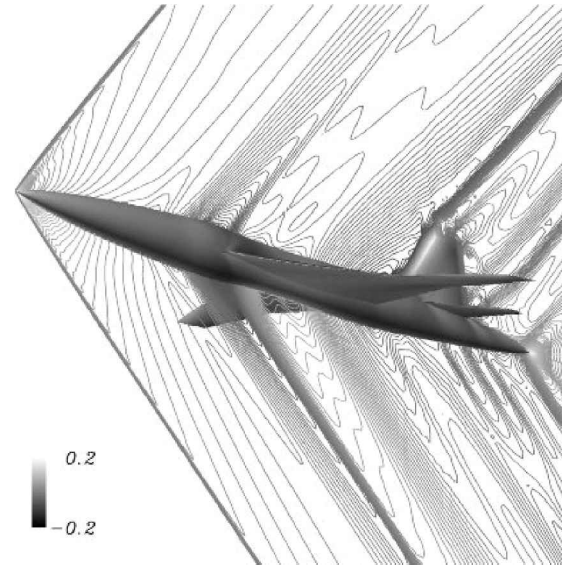

b) C_p contours

Fig. 5 CFD result for low-drag configuration without nacelles.

large as the Concorde and about 1/70 as heavy as the Concorde. The signatures for the other two configurations still keep non-N-shaped signatures on the ground, and the initial peak pressure levels are about 7.2 Pa smaller than that for the low-drag configuration. These two low-boom signatures, however, do not become exact flattop shape signatures because the flight altitude to the airplane length ratio for these scaled airplanes are too large ($H/L = 1250$). Therefore, the extrapolated signatures at $H/L = 300$, which seems to be suitable for a real size SST, are also shown in Fig. 6. The pressure signatures for low-boom and low-drag/low-boom configurations show more of a flattop-type shape, whereas that for the low-drag configuration has already become an N-shaped signature.

Figure 7 shows the drag polars ($C_{Dp} - C_L$ curves) for the configurations estimated by the CFD analyses. The curve for the low-boom configuration shifts upward by the axisymmetrical low-sonic-boom design from that for the low-drag configuration. The drag polar for the low-drag/low-boom configuration is located between the other two curves. Pressure drag coefficients at the flight condition ($C_L = 0.1$) and the sonic-boom intensities for these configurations are shown in Table 1. The drag of the low-boom configuration is 96 drag counts (1 drag count is $C_{Dp} = 0.0001$), which is 20 counts larger than that of the low-drag configuration. The

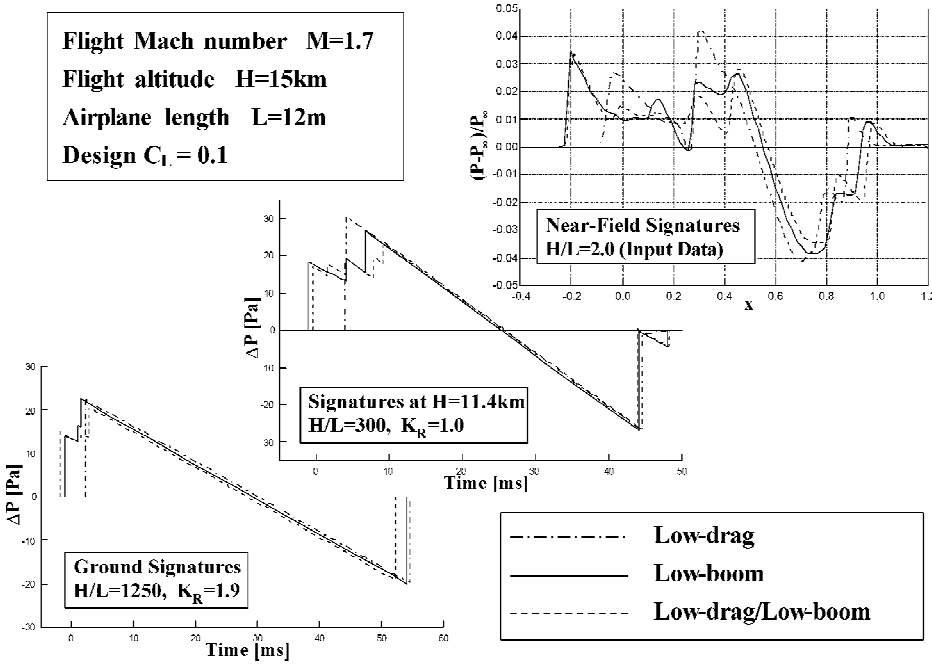

Fig. 6 Near-field and far-field pressure signatures for airplane configurations without nacelles.

Table 1 Characteristics for the configurations (without nacelles)

Configuration	Low drag	Low boom	Low drag/ Low boom
Fuselage volume, m^3	2.45	2.49	2.45
Pressure drag at design $C_L = 0.1$, counts	75.9	96.0	84.1
Sonic-boom intensity (initial pressure rise), Pa	22.5	13.9	14.8

nonaxisymmetrical fuselage design reduces the pressure drag of the low-boom configuration about 12 counts without increasing its sonic-boom intensity. The results show the effect of the nonaxisymmetrical fuselage design for reducing pressure drag of a low-sonic-boom airplane, although the pressure drag of the low-drag/low-boom configuration is still larger than that of the low-drag configuration about 8 counts.

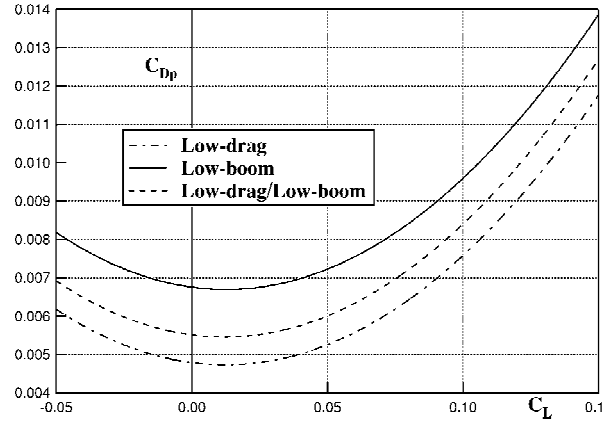

Fig. 7 Drag polars predicted by CFD analyses for airplane configurations without nacelles.

Airplane Configuration with Nacelles

Numerical Investigation

Next, the jet-powered experimental airplane shown in Fig. 1 is considered in the design of a low-sonic-boom configuration. In this case, the baseline configuration shown in Fig. 1 is called the low-drag configuration. The area distribution of this low-drag configuration shown in Fig. 8 is not an exact Sears–Haack body area distribution. In the design process of the low-drag configuration, first we designed an area-ruled configuration whose area distribution coincided with the Sears–Haack body shown by a dashed line in Fig. 8. The designed area-ruled fuselage has a very thick forebody because the areas of two large nacelles are concentrated in the rear part of the airplane. Therefore, we defined a slender fuselage shown in Fig. 1 to reduce the fuselage volume as long as the fuselage keeps the minimum radius at $x = 7$ m where the cross-sectional areas for two nacelles are very large. The drag prediction by a linear theory shows that the pressure drag of 115 counts for the low-drag configuration is smaller than that of 136 counts for the original area-ruled configuration. The CFD analysis is conducted for the low-drag configuration by the Euler CFD code with an overset grids technique.[10] The minor grid generated around a nacelle is overlapped to the main grid around a wing–body configuration as shown in Fig. 9a. The number of major grid points is the same as the earlier design case, and the number of minor grid points around a nacelle is about one million. The surface and near-field pressure contours around the low-drag configuration is

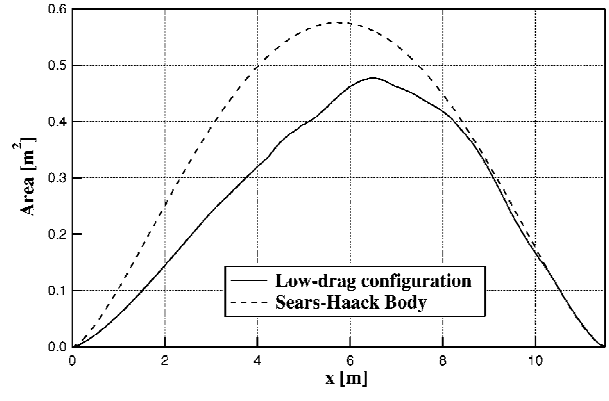

Fig. 8 Area distribution of low-drag configuration with nacelles.

shown in Fig. 9b. The equivalent area due to lift of the configuration is calculated by the CFD result and added to the area due to volume.

The total equivalent area distribution of the low-drag configuration is shown in Fig. 10. The design lift coefficient is determined from the flight condition of the scaled experimental airplane. For the low-boom design demonstration, it needs to fly as low as possible to generate a low-boom pressure signature on the ground. The lowest

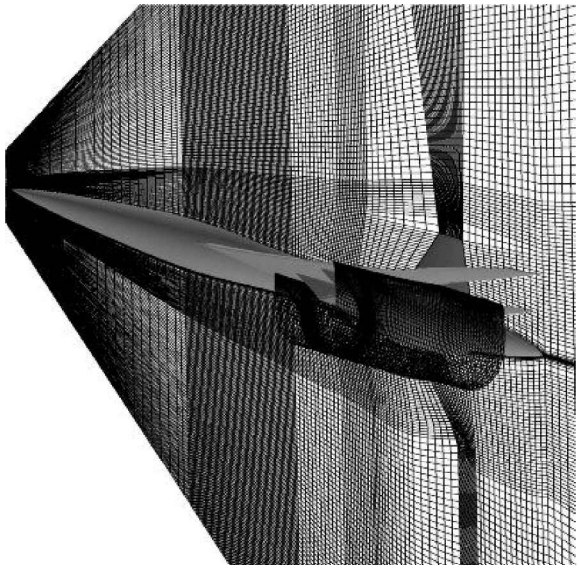

a) Overset grids

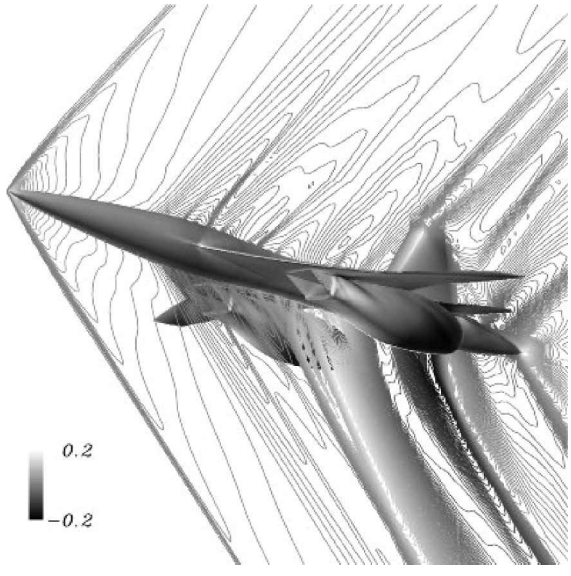

b) C_p contours

Fig. 9 CFD result for low-drag configuration with nacelles.

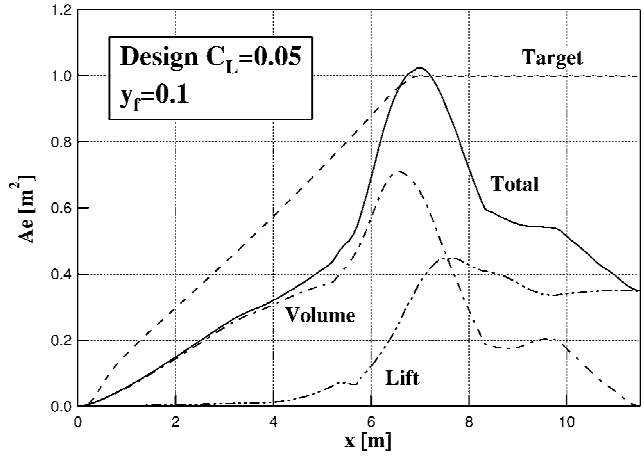

Fig. 10 Equivalent area distribution for low-drag configuration with nacelles.

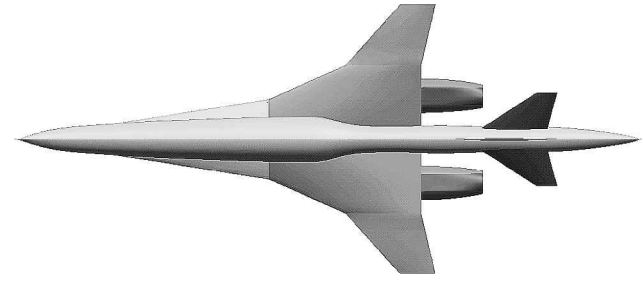

a) Top view

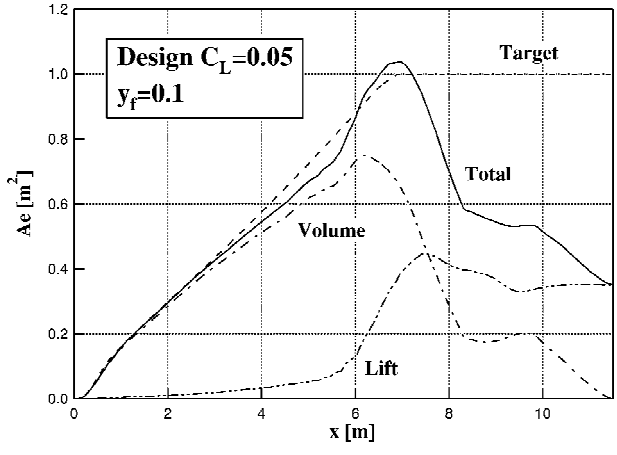

b) Equivalent area distribution

Fig. 11 Low-boom configuration with nacelles.

flight altitude determined from the structural limit of the experimental airplane at Mach 1.7 is about 11 km, and the airplane weight is about 2.5 tons. The design lift coefficient becomes $C_L = 0.05$, which seems to be smaller than that for the real SST. Therefore, the study in this case places emphasis on the verification of the nonaxisymmetrical fuselage design whose advantageous effects are shown in the preceding wing–body case. The peak value of the area distribution is about 1.0 m^2 at $x = 7$ m, and the target low sonic-boom area distribution shown in Fig. 10 is determined by Darden's method[3] so that its peak value becomes about the same as that of the low-drag configuration. Because the total equivalent area distribution and the target low-sonic-boom area distribution are quite different in the fore part, the low-boom configuration seems to have a very thick forebody to meet the target area distribution.

To avoid excessive volume increase, a wing strake as shown in Fig. 11a is added to the inner wing. Figure 11a shows the low-boom configuration with an axisymmetrical fuselage and Fig. 11b shows its total equivalent area distribution compared with the target low-sonic-boom area distribution. Although the equivalent area distribution due to lift of the low-boom configuration increases a little in the fore part compared with that of the low-drag configuration, the axisymmetrical forebody of the low-boom configuration is still very thick. The low-drag/low-boom configuration shown in Fig. 12a is designed by replacing the upper fuselage geometry of the low-boom configuration with that of the low-drag configuration. The side radius distribution of the low-drag/low-boom configuration, however, remains the low-boom geometry in the nose part of the fuselage, and it is smoothly connected to the low-drag side radius distribution on the upper side of the strake. The total area distribution of the low-drag/low-boom configuration shown in Fig. 12b becomes different from the target because of the decrease of area due to volume by cutting the upper side of the fuselage. It means that this low-drag/low-boom configuration is not a low-sonic-boom designed airplane anymore in linear theory. Therefore, only the nonlinear analyses using CFD or wind-tunnel tests can indicate that this configuration maintain low-boom characteristics. The differences among these three configurations are clearly seen in the front views shown in Fig. 13. The low-drag/low-boom configuration has the thin upper side fuselage the same as that of the low-drag configuration, and the thick lower side fuselage, the same as that of the low-boom configuration.

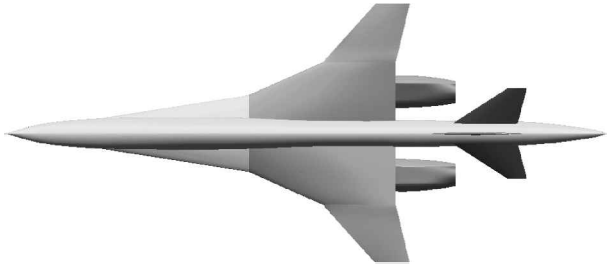

a) Top view

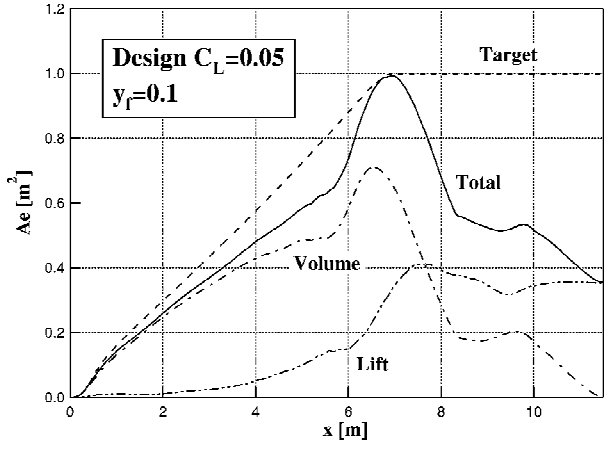

b) Equivalent area distribution

Fig. 12 Low-drag/low-boom configuration with nacelles.

a) Low-drag configuration

b) Low-boom configuration

c) Low-drag/low-boom configuration

Fig. 13 Front views.

The drag polars for the three configurations predicted by the Euler CFD analyses are shown in Fig. 14. The drag polar for the low-boom configuration shifts about 50 counts upward from that for the low-drag configuration. On the other hand, the pressure drag level of the low-drag/low-boom configuration is about the same as that of the low-drag configuration, although its fuselage volume is much larger than that of the low-drag configuration shown in Table 2.

Table 2 Characteristics for the configurations (with nacelles)

Configuration	Low drag	Low boom	Low drag/ Low boom
Fuselage volume, m^3	2.16	3.33	2.81
Wetted area, m^2	51.1	54.5	53.7
Pressure drag (CFD) at design $C_L = 0.05$, counts	137.7	187.2	136.8
Drag (measurement) at design $C_L = 0.05$, counts	285.2	338.6	286.7
Sonic-boom intensity (initial pressure rise), Pa	41.7	38.8	38.3

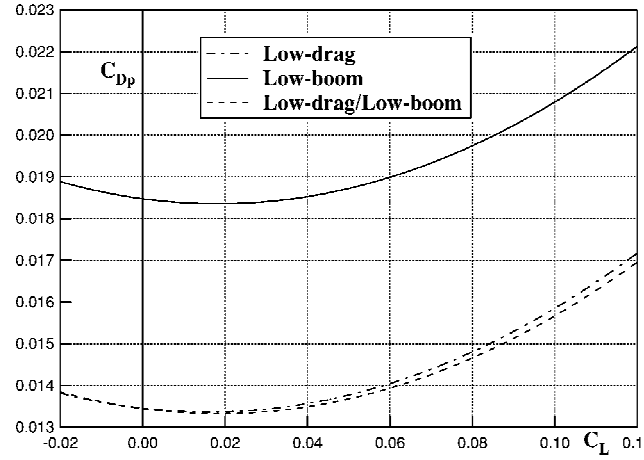

Fig. 14 Drag polars predicted by CFD analyses for airplane configurations with nacelles.

The predicted near-field pressure signatures at $H/L = 2.0$ under the airplane for the configurations are shown in Fig. 15. A high peak due to the nacelle shocks is shown in the signature for the low-drag configuration. The near-field pressure signatures for the low-boom and low-drag/low-boom configurations are very similar. Although the pressure peaks due to the nose shock for these two configurations are larger than that for the low-drag configuration, the pressure peaks due to the nacelle shocks are smaller than that for the low-drag configuration. The pressure signatures at $H/L = 150$ and on the ground extrapolated from these near-field pressure signatures are also shown in Fig. 15 in the flight condition of the scaled experimental airplane. The pressure signatures for the low-boom and low-drag/low-boom configurations at $H/L = 150$ keep non-N-shaped signatures, whereas that for the low-drag configuration becomes an N-shaped signature. On the other hand, the ground signatures show typical N-shape for all three configurations not only due to the large flight altitude to airplane length ratio ($H/L = 956$) but also due to the strong nacelle shocks that cannot be canceled by the expansion waves from the thick lower side fuselages. The initial pressure rises of the low-boom and low-drag/low-boom configurations, however, are about the same value of 38.8 Pa (0.8 psf), which is smaller than that of the low-boom configuration of 41.7 Pa (0.87 psf) as shown in Table 2. These numerical analyses show the nonaxisymmetrical fuselage design can reduce the pressure drag level of a low sonic-boom airplane without losing its low-sonic-boom characteristics.

Experimental Verification

Although the pressure drag of the low-drag/low-boom configuration predicted by the Euler CFD analysis at design lift coefficient ($C_L = 0.05$) is about 1 count smaller than that of the low-drag configuration, the wetted area of the low-drag/low-boom configuration is larger than that of the low-drag configuration due to the thick lower side fuselage as shown in Table 2. When the friction drag is considered, the verification of the nonaxisymmetrical fuselage design by wind-tunnel tests is needed. We conducted some wind-tunnel tests

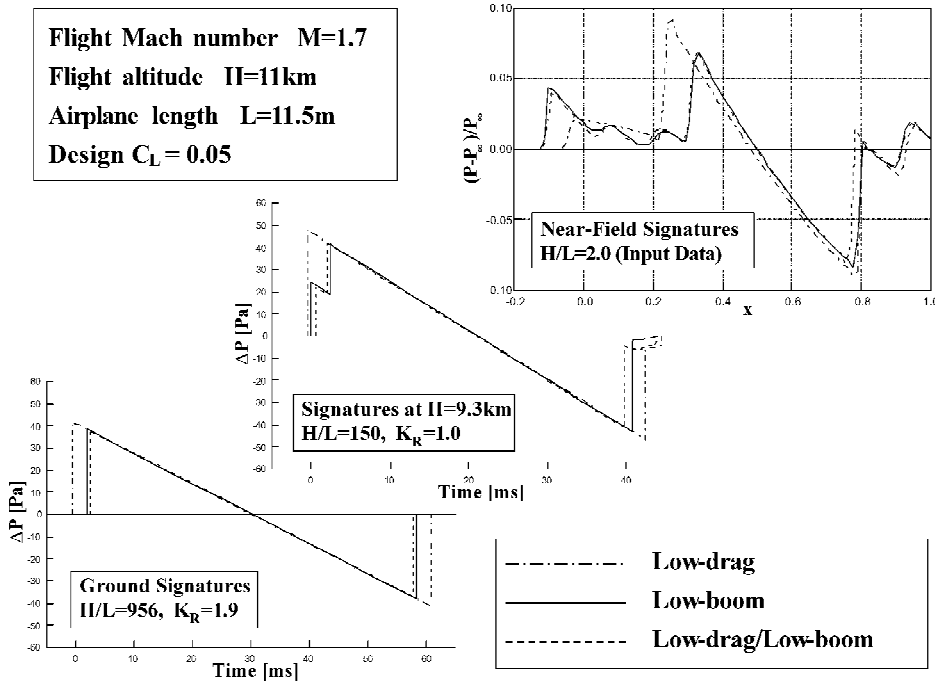

Fig. 15 Near-field and far-field pressure signatures for airplane configurations with nacelles.

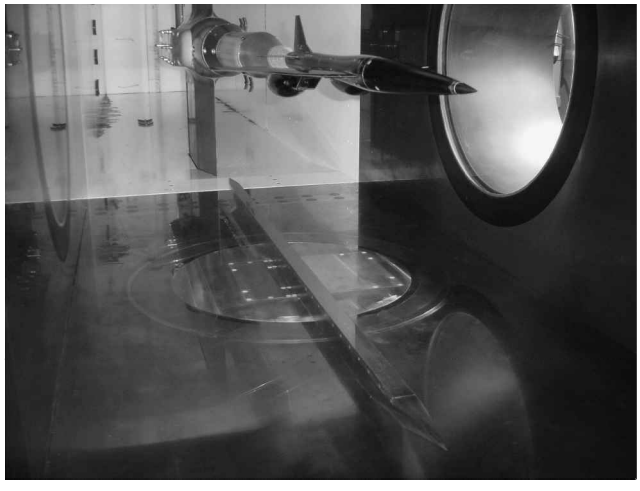

Fig. 16 Wind-tunnel test.

for these three configurations in NAL's supersonic wind tunnel. This wind tunnel is blowdown type, and its test section is 1 × 1 m square.

A schematic view of the test is shown in Fig. 16 in which the low-drag configuration model is set to the sting. In the tests, aerodynamic forces are measured by an internal six component balance, and near-field pressure signatures are measured by a 1.8-m-long pressure rod installed on the lower wind-tunnel wall. The pressure rod has about 300 static pressure taps in line on its upper surface. This 5-cm high pressure rod avoids the shock–boundary-layerinterference on the wind-tunnel wall, and its sharp nose prevents strong shock–shock interaction. The measured near-field pressure signatures in the freestream condition without wind-tunnel models are subtracted from the measured pressure signatures with models to eliminate the influences of the pressure rod itself. The results of the force measurements of three configurations compared with the CFD results are shown in Fig. 17. The measured C_L–α curves for three configurations are slightly different from those predicted by CFD analyses. In the CFD analysis, the C_L–α curve for the low-boom configuration is similar to that of the low-drag configuration. On the other hand, the C_L–α curve for the low-boom configuration is similar

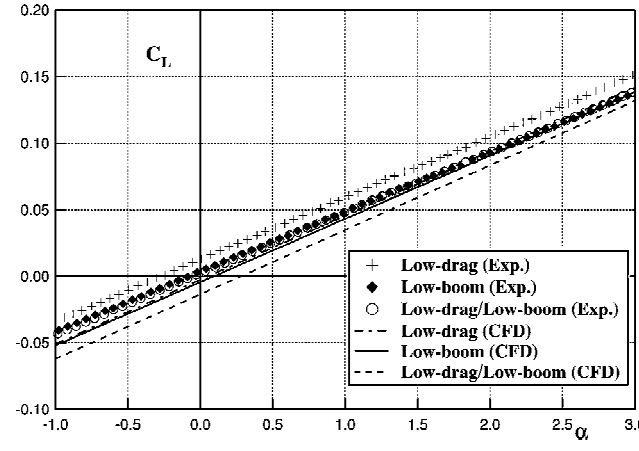

a) C_L–α

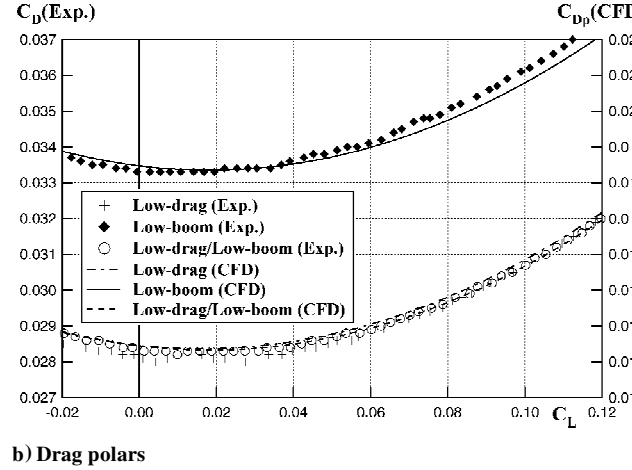

b) Drag polars

Fig. 17 Drag polars measured in wind-tunnel tests compared with CFD results.

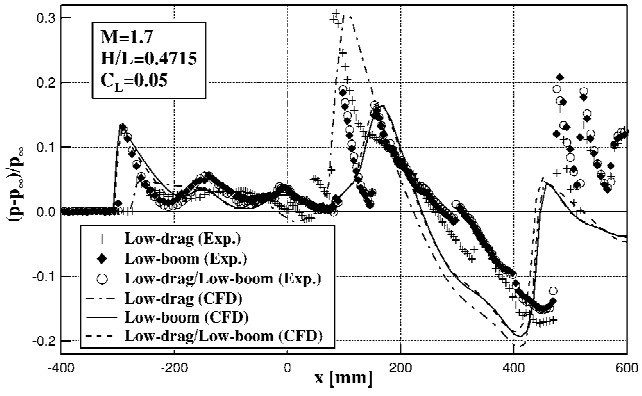

a) Under the airplane

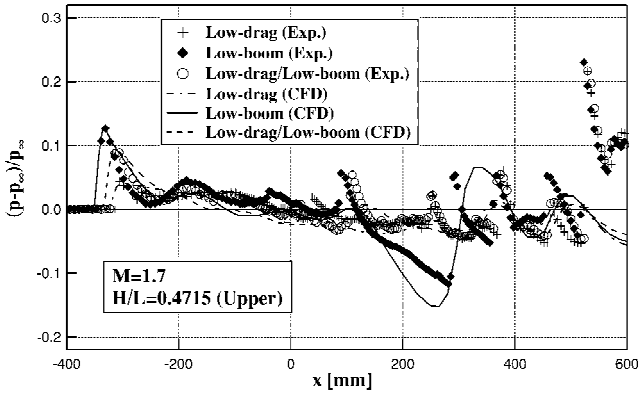

b) Above the airplane

Fig. 18 Measured near-field pressure signatures compared with CFD results.

to that of the low-drag/low-boom configuration in the wind-tunnel tests. This suggests that a certain phenomenon, which cannot be taken into account in the Euler CFD analysis, such as a separation, could occur in the flow around the low-boom configuration. The shapes of the drag polars for the configurations are similar to the CFD results, although the absolute values of drag coefficients are about 150 counts larger than those of CFD results due to the friction drag. The differences between the measured drag coefficients of the low-drag and low-boom configurations are about 53 counts, which are larger than the CFD results. The measured drag coefficient of the low-drag/low-boom configuration at design C_L becomes 1.5 counts larger than that of the low-drag configuration because of the friction drag.

The near-field pressure signatures measured at $H/L = 0.4715$ under the model compared with CFD results are shown in Fig. 18a. The signatures for the low-boom and low-drag/low-boom configurations are very similar. They show spiked shapes at the beginning of the signatures, which are the features of the low-sonic-boom near-field pressure signature. Their pressure peaks at $x = 100$ mm due to nacelle shocks are lower than that of the low-drag configuration. The signatures at $H/L = 0.4715$ above the model, which are measured by rotating the model upside down, are shown in Fig. 18b. The signature for the low-drag/low-boom configuration at this position is similar to that for the low-boom configuration in the fore part and is similar to that for the low-drag configuration in the rear part. In both graphs (Figs. 18a and 18b), the near-field pressure signatures predicted by CFD analyses show good agreement with the experimental data. The results of these wind-tunnel tests verify the effects of the nonaxisymmetrical design for reducing the drag of a low-sonic-boom configuration with an axisymmetrical fuselage without losing its low-sonic-boom characteristics, at least in the near-field of an airplane.

Conclusions

The nonaxisymmetrical fuselage shape modification of a low-sonic-boom airplane for reducing the drag is investigated by numerical analyses and is verified by wind-tunnel tests. The scaled supersonic airplane, which is designed for low drag and low boom using a nonaxisymmetrical fuselage, is compared with a conventional low-drag configuration and a low-boom configuration with an axisymmetrical fuselage. The numerical and experimental results show the design concept is effective for reducing the airplane drag without losing low sonic-boom characteristics.

Acknowledgments

The authors thank Fumitake Kuroda and the staff of the supersonic wind tunnel at the National Aerospace Laboratory Wind Tunnel Technology Center for their cooperation and assistance.

References

[1]Sakata, K., "Supersonic Experimental Airplane Program in NAL (NEXST) and Its CFD-Design Research Demand," *International Workshop on Numerical Simulation Technology for Design of Next Generation Supersonic Civil Transport*, SP-49T, National Aerospace Lab., Tokyo, 2000, pp. 53–56.

[2]Seebass, R., and George, A. R., "Sonic-Boom Minimization," *Journal of the Acoustical Society of America*, Vol. 51, Pt. 3, No. 2, 1972, pp. 686–694.

[3]Darden, C. M., "Sonic-Boom Minimization with Nose-Bluntness Relaxation," NASA TP-1348, Jan. 1979.

[4]Whitham, G. B., "The Flow Pattern of a Supersonic Projectile," *Communications in Pure and Applied Mathematics*, Vol. 5, 1952, pp. 301–348.

[5]Walkden, F., "The Shock Pattern of a Wing–Body Combination, Far from the Flight Path," *Aeronautical Quarterly*, Vol. 9, No. 2, 1957, pp. 164–194.

[6]Makino, Y., Iwamiya, T., and Lei, Z., "Fuselage Shape Optimization of a Wing–Body Configuration with Nacelles," *Journal of Aircraft*, Vol. 40, No. 2, 2003, pp. 297–302.

[7]Makino, Y., Aoyama, T., Iwamiya, T., Watanuki, T., and Kubota, H., "Numerical Optimization of Fuselage Geometry to Modify Sonic-Boom Signature," *Journal of Aircraft*, Vol. 36, No. 4, 1999, pp. 668–674.

[8]Makino, Y., and Iwamiya, T., "Numerical Simulation and Aerodynamic Design of an SST Configuration with Nacelles," AIAA Paper 2000-0126, Jan. 2000.

[9]Thomas, C. L., "Extrapolation of Sonic Boom Pressure Signatures by the Waveform Parameter Method," NASA TN D-6832, June 1972.

[10]Benek, J. A., Buning, P. G., and Steger, J. L., "A 3-D Chimera Grid Embedding Technique," *Proceedings of the 7th AIAA Computational Fluid Dynamics Conference*, AIAA, New York, 1985, pp. 322–331.

A. Plotkin
Associate Editor